Improved photoluminescence behavior of Eu^{3+}-activated $Ca_5(PO_4)_3F$ red nanophosphor by adding Li^+, Au^{3+}, and Bi^{3+} as co-dopants

Yumei Wu (吴玉梅)[1], Xuhui Xu (徐旭辉)[1,2], Xue Yu (余 雪)[1,2*], Buhao Zhang (张步豪)[1], Qianyue Li (黎千跃)[1], and Jianbei Qiu (邱建备)[1,2]

[1]*College of Materials Science and Engineering, Kunming University of Science and Technology, Kunming 650093, China*

[2]*Key Laboratory of Advanced Materials of Yunnan Province, Kunming University of Science and Technology, Kunming 650093, China*

[*]*Corresponding author: yuyu6593@126.com*

Received April 16, 2014; accepted July 3, 2014; posted online September 18, 2014

A series of $Ca_{4.99}(PO_4)_3F$:1%Eu^{3+}, 1%X (X = Li^+, Au^{3+}, and Bi^{3+}) nanoparticles are prepared using hydrothermal method, with an average size of 33–62 nm. We study the improved photoluminescence properties of $Ca_{4.99}(PO_4)_3F$:1%Eu^{3+} by co-doping with Li^+, Au^{3+}, and Bi^{3+} ions, respectively, and the enhancement of the emission intensities of Eu^{3+} is observed in these samples. The effects of Li^+ acting as a charge compensator, Au^{3+} as a plasma surface sensitizer, and Bi^{3+} as an energy conversion agent are discussed. The results show $Ca_{4.99}(PO_4)_3F$:1%Eu^{3+}, 1%X nanoparticles are a promising candidate as a red component for near-ultraviolet light-emitting diodes.

OCIS codes: 160.0160, 230.0230, 300.0300.

doi: 10.3788/COL201412.101602.

Over the past decades, many efforts have been made to study the photoluminescence properties of red phosphors for their applications in the fields of illuminations and displays, such as field emission displays, plasma display panels, white light-emitting diodes (LEDs), high-pressure fluorescent mercury lamps, color television cathode ray tubes, and so on[1]. For example, YVO_4:Eu^{3+} red phosphor has been widely used in color television cathode ray tubes[2]; (Y, Gd)BO_3:Eu^{3+} is the most widely used red-emitting borate phosphor for plasma display panel (PDP)[3]. And recently, much attention has been focused on nanophosphor. Comparing with the normal bulk phosphors, nano-sized phosphors usually exhibit novel capabilities, depending on their structure, shape, and size, such as tunable wavelengths[4], rapid responsibilities[5], and high efficiencies[6]. Besides, it was found that for the YVO_4:Eu^{3+} nanophosphors, the higher packing density and better paste rheology of smaller sized phosphors particles led to higher screen resolution and lower screen load[7,8]. However, there are still some drawbacks of these red phosphors with nano-scale, such as La_2O_2S:Eu^{3+}, which lacks chemical stability and produces decomposition products and is moisture sensitive[9]; (Y, Gd)BO_3:Eu^{3+} and YVO_4:Eu^{3+} nanoparticles, have higher color purity but exhibit lower luminescent intensity[10]. Therefore, a stable and high-efficient red-emitting nanophosphor still needs to be developed to satisfy the requirements of applications.

$M_5(PO_4)_3X$ (M = alkaline earths, X = halogens or OH) type of apatite materials are well-known for their applications as phosphor materials, laser hosts, and biocompatible materials[11]. It is known that $Ca_5(PO_4)_3F$ (FAP) is a good host lattice for luminescence and laser materials[12]. However, the growth of the single crystal of FAP is difficult and expensive[13]. Besides, the luminescence intensities are pretty low, such as $Ca_5(PO_4)_3$(F, Cl):Sb^{3+}, Mn^{2+} red phosphor, although their efficiency is high, the lumen equivalent of their emission is low compared with daylight, especially when applying to red emission beyond 610 nm, where the eye sensitivity is low[14].

Trivalent rare-earth (RE^{3+}) ion-doped luminescent materials receive constant attention due to their extensive applications[15], and Eu^{3+} ions have been extensively applied as red-emitting centers, such as (YVO_4):Eu^{3+}[8], (Y,Gd)(P,V)O_4:Eu^{3+}, Bi^{3+}[1],Gd_2O_3:Eu^{3+}[16], $CaYAl_3O_7$:Eu^{3+}[17], and $BaZr(BO_3)_2$:Eu^{3+}[3] red phosphor. In order to enhance the luminescence intensity of Eu^{3+}, different approaches were employed to achieve this purpose. For example, a significant change of morphology induced by an addition of a small amount of Li^+ could strongly enhance the cathodoluminescence efficiency of Gd_2O_3:Eu^{3+} phosphor[15]. Doping Bi^{3+} and Gd^{3+} can increase the efficiency of emission intensity of (P, V)O_4:Eu^{3+}, Bi^{3+} red nanophosphors at 619 nm under 365 nm excitation[1].

Here a series of nano-sized $Ca_{4.99}(PO_4)_3F$:1%Eu^{3+}, 1%X (X = Li^+, Au^{3+}, and Bi^{3+}) red phosphors were prepared by a simple hydrothermal method, which can be synthesized only by $Ca(CH_3COO)_2 \cdot 2H_2O$, Eu_2O_3, $(NH_4)_2HPO_4$, and CaF_2, and the improvement of photoluminescence properties was investigated by adding the same amount of Li^+, Au^{3+}, and Bi^{3+} with Eu^{3+}. The effects of Li^+, Au^{3+}, and Bi^{3+} ions co-doping on the enhancement of the characteristic emission

of Eu^{3+} were discussed separately. The nano-sized $Ca_{4.99}(PO_4)_3F$:1%Eu^{3+} red phosphor showed potential application for near-ultraviolet (near-UV) LEDs.

$Ca_{4.99}(PO_4)_3F$:1%Eu^{3+}, 1%X (X = Li^+, Au^{3+}, and Bi^{3+}) samples were prepared by the hydrothermal method. In a typical procedure, $Ca_{4.99}(PO_4)_3F$:1%Eu^{3+}, 1%Li^+ was selected as representative. Firstly, 0.015 mmol Eu_2O_3 was added into dilute HNO_3 solution and the 0.5 pH value was maintained, after the residual HNO_3 was heated and evaporated, 25 mL distilled water was poured into it to form a clear solution of $Eu(NO_3)_3$. Secondly, 1.5 mmol CaF_2, 13.47 mmol $Ca(CH_3COO)_2 2H_2O$, and 9 mmol $(NH_4)_2HPO_4$ were added to 25 mL distilled water with vigorous magnetic stirring at room temperature until it forms an aqueous solution. Subsequently, $Eu(NO_3)_3$ solution and 0.03 mmol $LiNO_3$ were separately added into the aqueous solution with vigorous stirring at room temperature to form a uniform and steady solution, and the pH was adjusted to be 5. Thirdly, the mixture was transferred into the Teflon bottle of a stainless autoclave to be heated at 180 °C for 16 h. After cooling down to room temperature naturally, the resultant products were collected by filtration, and the final products were synthesized after being heated in air at 800 °C for 2 h. The other samples were prepared by the similar procedure, except that $LiNO_3$ was free or replaced by colloidal gold and $Bi(NO_3)_3 \cdot 5H_2O$, respectively.

The structural characteristic of the final products were examined by powder X-ray diffraction (XRD) pattern using Cu-Kα (λ = 0.15405 nm) radiation on a diffractometer (Dmax 2500, Rigaku). The morphology and the size of the samples were inspected using a scanning electron microscope (SEM, S-4800, Hitachi) and transmission electron microscopy (TEM, G2-F20, American FEI). The excitation and emission spectra were obtained using a fluorescence spectrophotometer (F-7000, Hitachi). The room temperature decay curves were recorded using a spectrofluorometer (FLS920T, Edinburgh Instrument). All the measurements were carried out at room temperature.

Figure 1 shows the powder XRD patterns of $Ca_{4.99}(PO_4)_3F$:1%Eu^{3+}, 1%X (X = Li^+, Au^{3+}, and Bi^{3+}) phosphors. All the diffraction peaks can be indexed to pure hexagonal-structured $Ca_5(PO_4)_3F$ (JCPDS card no. 15-0786) with the space group of P63/m (no. 176). Their average size can be estimated by the Debye–Scherrer's equation[18]:

$$D = K\lambda/\beta\cos\theta,$$

where D represents the average diameter of the particles, K= 0.89, λ is the wavelength of the Cu-Kα radiation, θ is the Bragg angle, and β is the corrected full-width at half-maximum (FWHM). The calculated average sizes of $Ca_{4.99}(PO_4)_3F$:1%Eu^{3+}, 1%X (X = Bi^{3+}, Au^{3+}, Eu^{3+}, and Li^+) were 33.1, 55.4, 40.67, and 61.5 nm, respectively.

The morphologies and microstructures of the as-synthesized $Ca_{4.99}(PO_4)_3F$:1%Eu^{3+}, 1%X (X = Li^+ and Au^{3+}) samples were investigated by SEM and TEM, as shown in Fig. 2. All the samples had a regular and uniform morphology. From the TEM, we can see that phosphor consisted of some mono-disperse and uniform nanoparticles, and the average size of $Ca_{4.99}(PO_4)_3F$:1%Eu^{3+} particles is about 40 nm, and the grain size of $Ca_{4.99}(PO_4)_3F$:1%Eu^{3+}, 1%X (X = Li^+ and Au^{3+}) phosphors increased obviously compared with the $Ca_{4.99}(PO_4)_3F$:1%Eu^{3+}, which was consistent with the XRD results. Especially for the $Ca_{4.99}(PO_4)_3F$:1%Eu^{3+}, 1%Li^+ phosphor, not only the grain size increased much but also the crystallization property improved greatly. Due to the increasing size and improving crystallization property, we assume that Li^+ ion may also act as co-solvent in the $Ca_{4.99}(PO_4)_3F$:1%Eu^{3+}, 1%Li^+ phosphor.

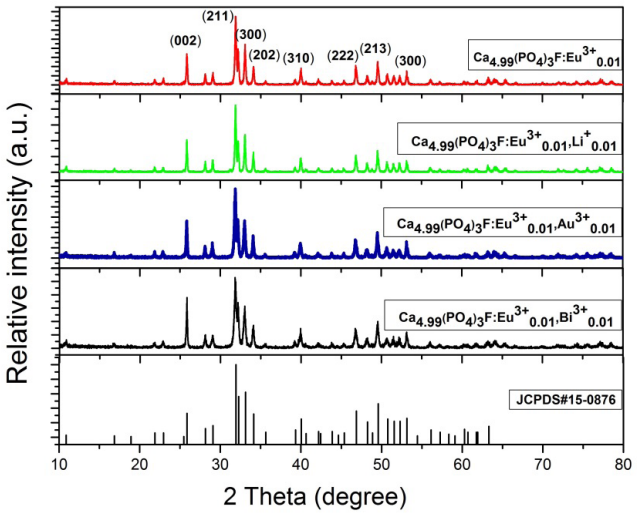

Fig. 1. XRD patterns of the $Ca_{4.99}(PO_4)_3F$:1%Eu^{3+}, 1%X (X = Li^+, Au^{3+}, and Bi^{3+}).

The excitation and emission spectra of $Ca_{4.99}(PO_4)_3F$:1%Eu^{3+}, 1%X (X = Au^{3+} and Li^+) nanoparticles were investigated, as shown in Figs. 3(a) and (b), respectively. It can be seen from Fig. 3(a) that the strongest excitation band of Eu^{3+} is at 393 nm, corresponding to the $^7F_0 \rightarrow {}^5L_6$ transition of Eu^{3+} ions. Figure 3(b) shows the emission peaks of Eu^{3+} at about 594, 619, and 655 nm which are attributed to the $^5D_0 \rightarrow {}^7F_1$, $^5D_0 \rightarrow {}^7F_2$, and $^5D_0 \rightarrow {}^7F_3$ transitions of Eu^{3+},

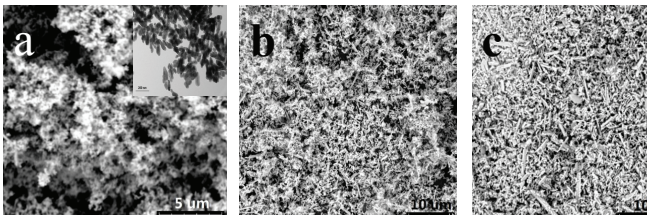

Fig. 2. SEM and TEM images of $Ca_{4.99}(PO_4)_3F$:1%Eu^{3+}, 1%X (X = Li^+ and Au^{3+}) samples: (a) $Ca_{4.99}(PO_4)_3F$:1%Eu^{3+} phosphor, and the inset is the TEM of $Ca_{4.99}(PO_4)_3F$:1%Eu^{3+}, (b) $Ca_{4.99}(PO_4)_3F$:1%Eu^{3+}, 1% Au^{3+} phosphor, and (c) $Ca_{4.99}(PO_4)_3F$:1%Eu^{3+}, 1% Li^+ phosphor.

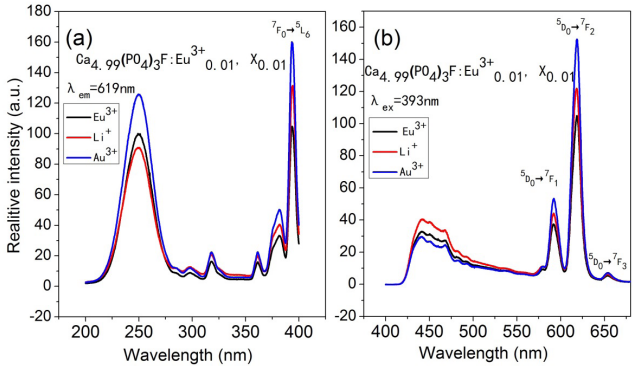

Fig. 3. Excitation and emission spectra of $Ca_{4.99}(PO_4)_3F$:1%Eu^{3+}, 1%X (X=Li^+ and Au^{3+}) nanoparticles.

respectively[11]. It can be seen that the shapes of the excitation and emission spectra of $Ca_{4.99}(PO_4)_3F$:1%Eu^{3+}, 1%X (X = Au^{3+} and Li^+) have no change compared with $Ca_{4.99}(PO_4)_3F$:1%Eu^{3+}, but the emission intensities improved greatly. From Figs. 3(a) and (b), the emission intensity of $Ca_{4.99}(PO_4)_3F$:1%Eu^{3+}, 1%Li^+ enhanced much, but the excitation intensity at the 250 nm broad band which was attributed to the charge transfer band (CTB) transition arising from O^{2-} ion to Eu^{3+} ion reduced, whereas the characteristic excitation peaks of Eu^{3+} increased. Voort and Blasse suggested that in some calcium compounds the ions with intra-ionic transitions seem to show efficient luminescence if they have a positive effective charge, whereas ions with an interionic transition (charge transfer between $Eu^{3+}$and O^{2-}), shows weak luminescence. A positive effective charge gave rise to a large relaxation in the charge transfer state and a low q_{CT} (quantum efficiency of CTB) value[19,20]. Thus, we can draw a conclusion that the Li^+ ion plays the role of charge compensator and introduces a positive charge in the luminescence process of $Ca_{4.99}(PO_4)_3F$:1%Eu^{3+}, 1%Li^+. We knew that when trivalent Eu^{3+} ions were doped into the $Ca_5(PO_4)_3F$ host lattice, they would chemically nonequivalently substitute the Ca^{2+} sites. And excess positive charge in the lattice must be compensated to maintain the electroneutrality of these phosphors due to these nonequivalent substitutions. In this process, vacancy defects $\left[V''_{Ca}\right]$ will be produced. When adding Li^+ ion, Li^+ acting as a charge compensation ion, the vacancy defects of the phosphors decrease, as a result, the luminescence intensity increases. And it is obvious that the excitation intensity at 393 nm (f–f transition of Eu^{3+} ions) was much stronger than that of 250 nm. This can match the radiation of near UV-emitting InGaN-based LED chips[21], which shows that the phosphor has potential application in the UV-LED. However, for Au^{3+} co-doped sample, the intensity of excitation spectra increased entirely, so we thought the Au^{3+} acted as a plasma surface sensitizer in the luminescence process of $Ca_{4.99}(PO_4)_3F$:1%Eu^{3+}, 1% Au^{3+}. In the emission spectra, the intensity of the 439 nm broad band which was related to host matrix $Ca_5(PO_4)_3F$[12] decreased, but the characteristic emission peaks of Eu^{3+} increased, which means that Au^{3+} may also promote the energy transfer (ET) from the host to Eu^{3+}.

The excitation and emission spectra of $Ca_{4.99}(PO_4)_3F$:1%Eu^{3+}, 1%Bi^{3+}nanoparticles were also recorded, as shown in Figs. 4(a) and (b), respectively. It is worth pointing out that the excitation spectrum of $Ca_{4.99}(PO_4)_3F$:1%Eu^{3+}, 1%Bi^{3+} was different from that of $Ca_{4.99}(PO_4)_3F$:1%Eu^{3+}. When Bi^{3+} ions are introduced into the phosphors, some changes in the wavelength range below 300 nm can be observed in Figs. 3(a) and 4(a). A rather broad shoulder band appears at about 275 nm in Fig. 4(a). To clarify the difference, the emission and excitation spectra of $Ca_{4.99}(PO_4)_3F$:1%Bi^{3+} were also measured, as shown in Fig. 4(a). Under the excitation at 275 nm, only one broad emission band with peak at 395 nm is observed in $Ca_{4.99}(PO_4)_3F$:1%Bi^{3+}, which is attributed to the $^1S_0 \rightarrow ^3P_1$ transition of Bi^{3+}. Moreover, it was observed that the excitation spectra of Eu^{3+}overlapped with the emission spectra of Bi^{3+}. According to Dexter's theory[22], an ET from Bi^{3+} to Eu^{3+} in $Ca_5(PO_4)_3F$ could be expected. Besides, it can be discovered that the emission intensity of $Ca_{4.99}(PO_4)_3F$:1%Eu^{3+}, 1%Bi^{3+} is much stronger than that of $Ca_{4.99}(PO_4)_3F$:1%Eu^{3+} under 275 nm excitation in Fig. 4(b), which provides further evidence of the ET between Bi^{3+} and Eu^{3+}.

In order to further confirm the ET from Bi^{3+} to Eu^{3+} in $Ca_{4.99}(PO_4)_3F$:1%Eu^{3+}, 1%Bi^{3+} phosphor, the fluorescence lifetimes τ_{Bi} for Bi^{3+} were measured and are presented in Fig. 5 (λ_{ex} = 275 nm and λ_{em} = 395 nm). The values of the lifetime were obtained by integrating the decay curves of which the initial intensities were normalized. With Eu^{3+} co-doping, the value of τ_{Bi} decreased from 1.539 to 1.468 ms. This behavior further indicates that the ET is dominated by Bi^{3+}–Eu^{3+} transfer.

In conclusion, $Ca_{4.99}(PO_4)_3F$:1%Eu^{3+}, 1%X (X = Li^+, Au^{3+}, and Bi^{3+}) nanoparticles with an average size of 33–62 nm are successfully prepared by the hydrothermal method. The as-synthesized $Ca_{4.99}(PO_4)_3F$:1%Eu^{3+}, 1%X (X=Li^+, Au^{3+}, and Bi^{3+}) particles have a uniform

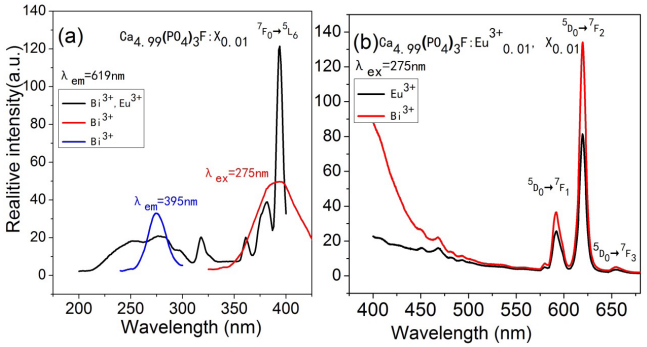

Fig. 4. Emission and excitation spectra of: (a) $Ca_{4.99}(PO_4)_3F$:1%X (X = Eu^{3+} and Bi^+) and (b) $Ca_{4.99}(PO_4)_3F$:1%Eu^{3+},1%X (X = Bi^+).

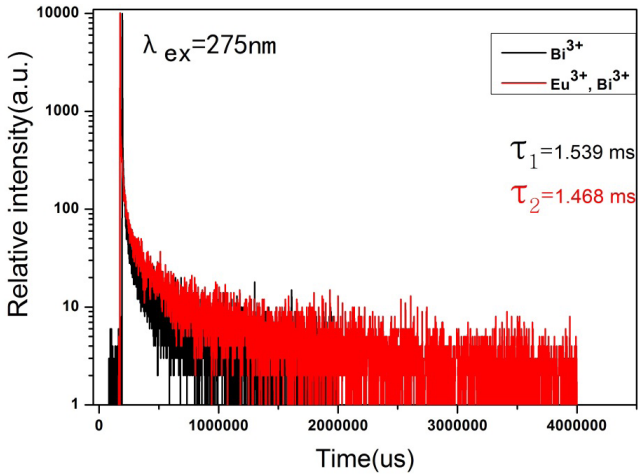

Fig. 5. Luminescence decay curves of $Ca_{4.99}(PO_4)_3F$:1%Eu^{3+}, 1% Bi^{3+} and $Ca_{4.99}(PO_4)_3F$:1%Bi^{3+} at 395 nm under 275 nm excitation.

and regular morphology. The addition of Li^+, Au^{3+}, and Bi^{3+} ions can increase the luminescence intensity of Eu^{3+} efficiently, and the influences of Au^{3+} acting as plasma surface sensitizer, Bi^{3+} ion as energy conversion agent, and Li^+ ion playing the role of charge compensator and co-solvent are studied. $Ca_{4.99}(PO_4)_3F$:1%Eu^{3+}, 1%X (X = Li^+, Au^{3+}, and Bi^{3+}) nanoparticles have potential applications in photoluminescence areas and NUV-LEDs.

This work was supported by the National Natural Science Foundation of China (No. 11204113), the Specialized Research Fund for the Doctoral Program of Higher Education of China (No. 20115314120001), and the Foundation of Natural Science of Yunnan Province (No. 2011FB022).

Reference

1. Y. Pu, K. Tang, D. C. Zhu, T. Han, C. Zhao, and L. L. Peng, Nano Micro Lett. **5,** 117 (2013).
2. F. C. Palilla, A. K. L. Levine, and M. Rinkevics, J. Electrochem. Soc. **112,** 776 (1965).
3. L. Tian, B. Y. Yu, C. H. Pyun, H. L. Park, and S. Mho, Solid State Commun. **129,** 43 (2004).
4. D. F. Wang, J. Wang, and P. X. Liu, Angew. Chem. **122,** 7618 (2010).
5. G. F. Wang, W. P. Qin, J. Zhang, J. S. Zhang, W. Yan, C. Y. Cao, L. L. Wang, G. D. Wei, P. F. Zhu, and R. J. Kim, J. Phys. Chem. C **112,** 12161 (2008).
6. R. N. Bhargava, D. Gallagher, X. Hong, and A. Nurmikko, Phys. Rev. Lett. **72,** 416 (1994).
7. D. S. Jo, Y. Y. Luo, K. Senthil, T. Massaki, and D. H. Yoon, Opt. Mater. **33,** 1190 (2011).
8. Q. Z. Dong, Y. H. Wang, L. L. Peng, H. J. Zhang, and B. T. Liu, Nanotechnol. **22,** 215604 (2011).
9. S. Neeraj, N. Kijima and A. K. Cheetham, Chem. Phys. Lett. **387,** 2 (2004).
10. K. Park and S. W. Nam, Mater. Chem. Phys. **123,** 601 (2010).
11. R. Sahoo, S. K. Bhattacharya, and R. Debnath, J. Solid State Chem. **175,** 218 (2003).
12. Z. L. Fu, X. J. Wang, Y. M. Yang, Z. J. Wu, D. F. Duan, and X. H. Fu, Dalton Trans. **43,** 2819 (2014).
13. R. Hopkins, D. Damon, P. Piotrowski, M. Walker, and J. Uphoff, J. Appl. Phys. **42,** 272 (1971).
14. C. Feldmann, T. Jüstel, C. R. Ronda, and P. J. Schmidt, Adv. Funct. Mater. **13,** 511 (2003).
15. L. Wang, C. Xia, P. Xu, J. Di, Q. Sai, and F. Mou, Chin. Opt. Lett. **11,** 061604 (2013).
16. J. C. Park, H. K. Moon, D. K. Kim, and S. H. Byeon, Appl. Phys. Lett. **77,** 2162 (2000).
17. H. Yu, X. Yu, X. Xu, Q. Jiao, T. Jiang, X. Liu, D. Zhou, and J. Qiu, Chin. Opt. Lett. **12,** 051602 (2014).
18. M. Yin and S. O'Brien, J. Am. Chem. Soc. **125,** 10180 (2003).
19. D. V. D. Voort and G. Blasse, J. Solid State Chem. **99,** 404 (1992).
20. D. V. D. Voort and G. Blasse, Chem. Mater. **3,** 1041 (1991).
21. F. Du, Y. Nakai, T. Tsuboi, Y. L. Huang, and H. J. Seo, J. Mater. Chem. **21,** 4669 (2011).
22. G. Blasse, Prog. Solid State Chem. **18,** 79 (1988).